

# Fractional quantum anomalous Hall effects in rhombohedral multilayer graphene in the moiréless limit and in Coulomb imprinted superlattice

Boran Zhou,<sup>1</sup> Hui Yang,<sup>1</sup> and Ya-Hui Zhang<sup>1</sup>

<sup>1</sup>*Department of Physics and Astronomy, Johns Hopkins University, Baltimore, Maryland 21218, USA*  
(Dated: November 27, 2023)

The standard theoretical framework for fractional quantum anomalous Hall effect (FQAH) assumes an isolated flat Chern band in the single particle level. In this paper we challenge this paradigm for the FQAH recently observed in the pentalayer rhombohedral stacked graphene aligned with hexagon boron nitride (hBN). We show that the external moiré superlattice potential is simply a perturbation in a model with continuous translation symmetry. Through Hartree Fock calculation, we find that interaction opens a sizable remote band gap, resulting in an isolated narrow  $C = 1$  Chern band at filling  $\nu = 1$ . From exact diagonalization (ED) we identify FQAH phases at various fillings. But they exist also in the calculations without any external moiré potential. We suggest that the QAH insulator at  $\nu = 1$  should be viewed as an interaction driven QAH-Wigner crystal, which is then pinned by a small moiré potential. In the second part we propose a new setup with Coulomb generated moiré superlattice. For example, we separate  $n$ -layer graphene and twisted bilayer graphene (TBG) with a thin hBN and imprint the superlattice of the TBG to the  $n$ -layer graphene. Now the superlattice potential is controlled by the thickness  $d$  of the hBN and the superlattice period is controlled by the twist angle of the TBG. Overall in both setups the  $C = 1$  QAH-Wigner crystal is robust with a crystal period around 10nm in 4-layer, 5-layer, 6-layer and 7-layer graphene systems. Our work suggests a new direction to explore the interplay of topology and FQAH with spontaneous Wigner crystal formation in the vanishing moiré potential limit.

**Introduction** There have been lots of efforts in realizing fractional quantum Hall (FQH) states[1, 2] from fractionally filling a narrow Chern band [3–11] on a lattice. Such a state is dubbed as fractional Chern insulator (FCI). FCI has been experimentally realized at non-zero magnetic field[12, 13]. Fractional quantum anomalous Hall effect (FQAH) phase, a FCI at zero magnetic field, is more challenging. It was proposed that the two dimensional moiré systems are wonderful platforms to host nearly flat Chern band and thus FQAH states[14–18] following spontaneous valley polarization[14, 19]. Indeed integer quantum anomalous Hall (QAH) states[20, 21] were realized in twisted bilayer graphene(TBG) aligned with hexagon boron nitride (hBN)[22, 23], in ABC stacked trilayer graphene moiré with hBN alignment[24], and also in transition Metal Dichalcogenide (TMD) bilayers[25, 26]. More recently, FQAH was finally observed in twisted MoTe<sub>2</sub> homobilayer from optical and capacitance measurement[27, 28], further supported directly from transport measurements[29, 30]. Theoretically the existence of the FQAH (zero field FCI) in the twisted MoTe<sub>2</sub> system is quite natural due to the existence of isolated narrow Chern band[31–33]. Indeed FQAH phases were predicted[34, 35] even before the experiment. Recent theoretical works further confirm the existence of FQAH [36–39] and also composite Fermi liquid (CFL)[40, 41] at even denominator. Apparently twisted MoTe<sub>2</sub> system mimics the familiar lowest Landau level physics quite well.

Possibility of FQAH was also discussed in graphene systems[14, 42–47], but so far it has been reported only in pentalayer (5-layer) rhombohedral stacked graphene aligned with hBN[48], which is actually a surprise and unexpected theoretically. In the following we always re-

fer  $n$ -layer graphene to rhombohedral stacked multilayer graphene. It was predicted by one of us[14, 49] that there is a  $C \neq 0$  band in  $n$ -layer graphene aligned with hBN for one sign of the displacement field  $D$ , corresponding to the side where particles are pushed away from the hBN. See also Ref. [50] for earlier discussions on possible narrow bands with non-zero Berry curvature in the system. The superlattice potential from the hBN alignment on top only applies on the top layer of the  $n$ -layer graphene. Therefore, for the topological side of  $D$ , electrons feel a weaker superlattice potential and the remote gap tends to be small. This effect is more severe for larger  $n_{\text{layer}}$  because  $D$  can polarize the layer degree of freedom more easily. For the 5-layer graphene, FQAH is found only in the strong displacement region and we estimate that the moiré superlattice potential projected to the conduction band is only at order of 0.05meV. Such a small superlattice potential is only a perturbation term and we indeed notice that the band structures with and without moiré potential are roughly the same. Hence it is a surprise that even QAH insulator can be stabilized at  $\nu = 1$  filling per moiré unit cell.

We resolve this puzzle by performing a Hartree Fock calculation at filling  $\nu = 1$  first. Assuming spin-valley polarization[19], we find a  $C = 1$  Chern insulator in a range of displacement field  $D$  at twist angle  $\theta \in (0.66^\circ, 1.47^\circ)$  with sizable band gap and narrow bandwidth of the filled band. Then at fractionally filling of the Hartree Fock (HF) renormalized band, we find FQAH insulators through exact diagonalization (ED). There is also signature of composite Fermi liquid[51] at 1/2 filling. In this calculation, the external moiré potential does not play any essential role. The same result can be reproduced by a calculation with the moiré potential turned

off by hand. In this sense, we should view the  $\nu = 1$  Chern insulator as a QAH Wigner crystal spontaneously breaking the approximate continuous translation symmetry, which is then pinned by the small external moiré potential. The FQAH is then realized at fractional filling of this spontaneously formed crystal. Our work thus establishes the  $n$ -layer graphene as a completely new platform for FQAH phase, distinct from twisted MoTe<sub>2</sub>. We note that the picture of viewing moiré as a perturbation has already been suggested in Ref.52 in the trilayer graphene system, though in that case there is still controversy and the main focus is on the valence band[53]. When the  $n_{\text{layer}} \geq 4$ , the conduction band is more flat and the projected moiré potential is clearly small, hence the physics is closer to the moiréless limit with approximate continuous translation symmetry. This implies that it may be possible even to realize the QAH Wigner crystal in the moiréless  $n$ -layer graphene[54–57]. Note that QAH Wigner crystal state has been suggested in experiment of bilayer graphene[58], though there still lacks unambiguous evidence of QAH effect there.

In the second part, we ask whether it is possible to generate a moiré superlattice potential on the  $n$ -layer graphene without hBN alignment. Especially it is desirable to tune the moiré superlattice potential continuously and control the superlattice period separately. We propose a new setup to achieve this by Coulomb induced superlattice. Specifically, we consider a system with  $n$ -layer graphene separated from a twisted bilayer graphene

$$\begin{aligned}
H_0 = & \sum_{\mathbf{k}} \sum_{z=1}^{n_{\text{layer}}} \psi_z^\dagger(\mathbf{k}) \begin{pmatrix} V_{z,l} + u_{A,l} & -v_1(k_x - ik_y)e^{i\theta_3} \\ -v_1(k_x + ik_y)e^{-i\theta_3} & V_{z,l} + u_{B,l} \end{pmatrix} \psi_z(\mathbf{k}) + \sum_{\mathbf{k}} \sum_{z=1}^{n_{\text{layer}}-2} \psi_z^\dagger(\mathbf{k}) \begin{pmatrix} 0 & \frac{\gamma_2}{2} \\ 0 & 0 \end{pmatrix} \psi_{z+2}(\mathbf{k}) + \text{H.c.} \\
& + \sum_{\mathbf{k}} \sum_{z=1}^{n_{\text{layer}}-1} \psi_z^\dagger(\mathbf{k}) \begin{pmatrix} -v_4(k_x - ik_y)e^{i\theta_3} & -v_3(k_x + ik_y)e^{-i\theta_3} \\ \gamma_1 & -v_4(k_x - ik_y)e^{i\theta_3} \end{pmatrix} \psi_{z+1}(\mathbf{k}) + \text{H.c.}
\end{aligned} \tag{1}$$

where the parameters  $v_i = \frac{\sqrt{3}}{2}t_i$ , with [59, 60]  $t_1 = -2600\text{meV}$ ,  $t_3 = 293\text{meV}$ ,  $t_4 = 144\text{meV}$ ,  $\gamma_1 = 358\text{meV}$ ,  $\gamma_2 = -8.3\text{meV}$  correspond to the hoppings.  $V_{z,l}$  is the layer-dependent potential from the displacement field with  $V_{z,l} = \frac{D(l-1-n_{\text{layer}}/2)}{n_{\text{layer}}-1}$ , where  $D$  is the displacement field, and  $l = 1, 2, \dots$  is the  $l$ -th layer.  $u_{A,1} = u_{B,n_{\text{layer}}} = 0$ ,  $u_{B,1} = u_{A,n_{\text{layer}}} = 12.2\text{meV}$ ,  $u_{A,l} = u_{B,l} = -16.4\text{meV}$  for other terms. The phase  $\theta_3$  is introduced to rotate the graphene. We have  $\theta_3 = \arctan \frac{\theta}{\delta}$  with  $\theta$  as the twist angle between graphene and hBN.  $\delta = \frac{a_{\text{hBN}} - a_{\text{G}}}{a_{\text{hBN}}} = 0.017$ ,  $a_{\text{G}}(0.246\text{nm})$  and  $a_{\text{hBN}}(0.25025\text{nm})$  are the lattice constant of graphene and hBN respectively.

The moiré potential term is  $H_M = \sum_{\mathbf{k}} \sum_{j=1}^6 \psi_1^\dagger(\mathbf{k}) H_M(\mathbf{G}_j) \psi_1(\mathbf{k} + \mathbf{G}_j)$  which only acts on the first layer aligned with the hBN. Here the moiré reciprocal lattice vectors are  $\mathbf{G}_j = \frac{4\pi}{\sqrt{3}a_M} (\cos(\frac{j\pi}{3} - \frac{5\pi}{6}), \sin(\frac{j\pi}{3} - \frac{5\pi}{6}))^T$ ,  $j = 1, 2, \dots, 6$ .

by a thin hBN. The  $n$ -layer graphene is misaligned with hBN, but it feels the moiré superlattice potential from the hBN by inter-layer repulsion. The moiré period  $a_M$  is controlled by the twist angle of TBG, which does not need to be close to the magic angle for our purpose. We will tune the density of TBG to be  $\nu_{\text{TBG}} = 4$  so it is in a band insulator. We find Chern insulator with narrow  $C = 1$  band at  $\nu = 1$  in a range of the parameter space  $(a_M, d, D)$  for  $n_{\text{layer}} = 4, 5, 6, 7$ . Now narrow  $C = 1$  band is possible in both signs of  $D$  for  $a_M \approx 10\text{nm}$ . The same idea works if we replace the TBG with a monolayer graphene aligned with the middle hBN. Given the large tunability of the system, we expect a rich phase diagram to be found in future experimental studies of this new class of moiré materials. Especially one can tune the moiré potential by the distance  $d$  to verify our conjecture that QAH and maybe even FQAH are possible in the zero moiré potential limit.

**Model** We model the  $n$ -layer graphene aligned with hexagonal boron nitride (hBN) as  $H_K = H_0 + H_M$ , where  $H_0$  is the Hamiltonian of  $n$ -layer graphene and  $H_M$  is the effective moiré potential from hBN alignment. It is by now well established that the  $\nu = 1$  QAH insulator is spin-valley polarized from the Coulomb exchange[19]. The real puzzle is how to obtain a Chern band within one spin-valley flavor. We will thus assume spin-valley polarization and focus on one valley and define  $\psi_z(\mathbf{k}) = (f_{z,A}(\mathbf{k}), f_{z,B}(\mathbf{k}))^T$  for the two sublattice at the layer  $z$ . Then the free Hamiltonian is written down as a  $2n_{\text{layer}}$  band model:

The moiré potential parameters are listed [59–61] in the supplementary. In the following we will also introduce a parameter  $V_M$  to scale the moiré potential term by  $H_M \rightarrow V_M H_M$ . We mainly focus on  $V_M = 1, 0$ .

In addition to the kinetic energy, we also have the Coulomb interaction:

$$H_V = \frac{1}{2A} \sum_{l,l'} \sum_{\mathbf{q}} V_{ll'}(\mathbf{q}) : \rho_l(\mathbf{q}) \rho_{l'}(-\mathbf{q}) : \tag{2}$$

where  $A$  is the area of the sample,  $\rho_l(\mathbf{q})$  is the density operator in the layer  $l$ .  $V_{ll'}(\mathbf{q}) = \frac{e^2 \tanh q\lambda}{2\epsilon_0 \epsilon q} e^{-q|l-l'|d_{\text{layer}}}$ ,  $\lambda = 30\text{nm}$  is the screening length and  $d_{\text{layer}} = 0.34\text{nm}$  is the distance between nearest two layers.

**Numerical evidence of QAH and FQAH** We focus on the conduction band on the large and negative  $D$ , so electrons in the conduction band are mainly staying in the bottom, far away from the aligned hBN on

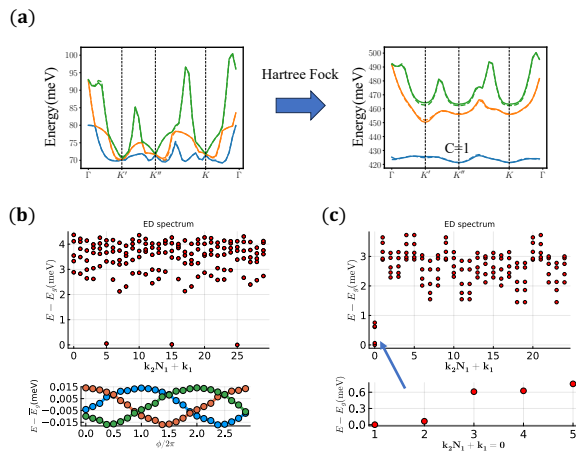


FIG. 1: Numerical results of the 5-layer graphene/hBN system at  $\theta = 0.77^\circ$  ( $a_M = 11.36\text{nm}$ ),  $\epsilon = 6$ ,  $D = -160\text{meV}$ . (a) Conduction band structure before and after performing HF approximation, the HF calculation is performed by using  $30 \times 30$  points in the moiré Brillouin zone (MBZ). The solid line and the dashed line corresponds to  $V_M = 1, 0$  respectively. They are basically identical to each other. (b) ED calculation at  $\nu = 2/3$  filling with a system size of  $5 \times 6$ . We project to the lowest band in the Hartree fock calculation using hole picture at hole filling  $\nu_h = 1 - \nu = 1/3$ . We use the dispersion of the band from the Hartree Fock calculation.  $k_1$  and  $k_2$  is defined as  $\mathbf{k} = k_1 \mathbf{G}_1/N_1 + k_2 \mathbf{G}_2/N_2$  with the system size of  $N_1 \times N_2$ . We also show the spectral flow under flux insertion along  $k_2$  direction. The flux insertion calculation is performed with system size of  $4 \times 6$ . Clearly there is a permutation of the degenerate states under a flux of  $\phi = 2\pi$ . (c) ED calculation at  $\nu = 3/5$  filling with system size  $5 \times 5$ . In the lower part we show a zoom in of the five nearly degenerate states.

the top. In Fig. 1(a) we can clearly see that there is no remote band gap for the 5-layer graphene at  $\theta = 0.77^\circ$ ,  $D = -160\text{meV}$ . Actually the band structure is basically the same as the band of the moiréless 5-layer graphene folded into the moiré Brillouin zone (MBZ). Then with a Hartree Fock calculation (see the supplementary) keeping the lowest  $N_b = 3$  number of conduction bands at the filling  $\nu = 1$  per moiré unit cell, we find a sizable band gap opening and a filled nearly flat  $C = 1$  band (see Fig. 1(a)). This means that the  $\nu = 1$  filling is an interaction driven QAH insulator. Then we perform exact diagonalization (ED) projected to the Hartree Fock renormalized lowest band. Note that we need to use the hole picture with Hartree-Fock renormalized dispersion relative to the fully filled band insulator. The electron picture is different due to the normal ordering of the interaction term. In Fig. 1(b)(c) we can see low lying 3-fold and 5-fold states, consistent with FCI at electron filling  $\nu = 2/3$  and  $\nu = 3/5$  respectively. At  $\nu = \frac{1}{2}$ , we also find signature of composite Fermi liquid (CFL) (see the

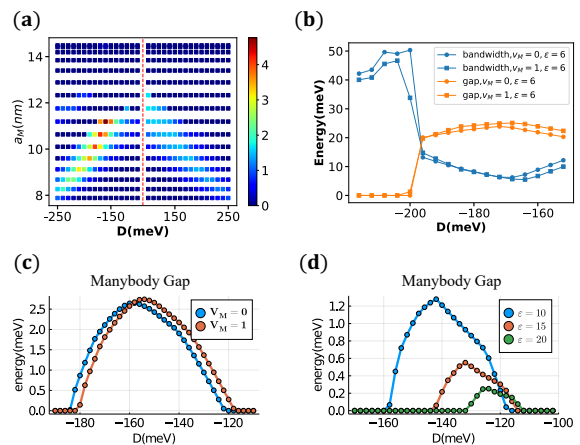


FIG. 2: The HF calculation is performed by using  $12 \times 18$  points in MBZ. (a)  $\epsilon = 6$ , dependence of  $\frac{|C|\Delta}{W}$  on  $D$  and the moire lattice constant  $a_M$ .  $|C|$  is the Chern number,  $\Delta$  is the band gap at filling  $n = 1$  and  $W$  is the band width of the lowest band after Hartree Fock. When  $a_M > 12\text{nm}$ , the  $C=1$  QAH crystal disappears. (b) At  $\theta = 0.9^\circ$  ( $a_M = 10.63\text{nm}$ ),  $\epsilon = 6$ , dependence of the Hartree Fock renormalized band gap and the bandwidth on  $D$ . (c) At  $\theta = 0.9^\circ$  ( $a_M = 10.63\text{nm}$ ),  $\epsilon = 6$ , dependence of the many body gap of the FQAH insulator at  $\nu = 2/3$  filling on  $D$ . The many body gap is defined as the energy difference between the fourth and the third states in the ED calculation. The ED calculation is performed by using  $4 \times 6$  points in MBZ. We have introduced a factor  $V_M$  to the moiré potential term  $H_M$ .  $V_M = 0$  means that the moiré potential is turned off. (d) Similar to (c), but with different value of  $\epsilon$  and  $V_M = 0$ .

supplementary).

**Phase diagram** Next we study the phase diagram in the  $(\theta, D)$  space for the 5-layer graphene/hBN system. In Fig. 2(a) we show a color map of  $\frac{|C|\Delta}{W}$  with  $C, \Delta, W$  as the Chern number, the band gap and the bandwidth from the Hartree Fock calculation at the filling  $\nu = 1$ . The phase diagram is dominated by  $|C| = 0, 1$ . We find that we always have  $C = 0$  for twist angle  $\theta < 0.65^\circ$ . The ideal region with large  $\frac{|C|\Delta}{W}$  is stabilized with  $a_M \in (8, 12)\text{nm}$ , corresponding to  $\theta \in (0.66^\circ, 1.47^\circ)$ .

In Fig. 2(b) we further check the existence of a narrow  $C = 1$  band with sizable band gap at  $\epsilon = 6$  and  $\theta = 0.9^\circ$ , with and without the moiré potential term. In Fig. 2(c) we show the corresponding many body gap of the FQAH at  $\nu = 2/3$ . One can see a dome of FQAH phase in a wide range of the displacement field  $D$ . We find  $\theta = 0.9^\circ$  is more ideal than  $\theta = 0.77^\circ$ . Interestingly, we find that  $V_M = 0$  and  $V_M = 1$  show basically the same result, implying that the moiré potential term is not important in our calculation. In Fig. 2(d) we show the many body gap at different dielectric constant  $\epsilon = 10, 15, 20$ . One can see the stable region of FQAH is diminished at larger

$\epsilon$ , but there is still a gap at order 0.2 meV at  $\epsilon = 20$ , which is actually closer to the experimental value.

**The role of the moiré potential** Our result in Fig. 2 clearly shows that the external moiré potential term is not essential for QAH and FQAH phases in this system. We project the moiré potential into the conduction band, the matrix element is around 0.03meV and 0.05meV at  $K, K'$  points respectively, which is obviously just a tiny perturbation. Therefore, we conclude that the narrow Chern band shown in Fig. 1(a) is completely from the Coulomb interaction. Our  $\nu = 1$  QAH insulator survives to the  $V_M \rightarrow 0$  limit and should be viewed as a Wigner crystal spontaneously breaking the continuous translation symmetry. The FQAH phases are then realized at fractional filling of this crystal. The external moiré potential may still be necessary to pin the crystal and stabilize the FQAH phases, but it plays no roles in producing the narrow Chern band. It is interesting to see whether a QAH Wigner crystal can be realized in a really moiréless system in future experimental investigations.

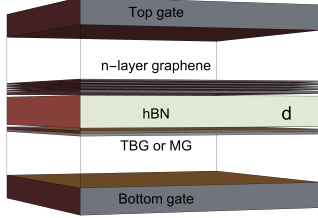


FIG. 3: Illustration of the  $n$ -layer graphene/hBN/TBG setup. The Coulomb interaction between the TBG and the  $n$ -layer graphene will effectively generate a moiré potential in the  $n$ -layer graphene. We fix the density of TBG in the fully filled filling  $\nu_{\text{TBG}} = 4$ . The TBG can also be replaced with a monolayer graphene (MG) aligned with the middle hBN.

**Coulomb induced moire** In the second part, we propose a different route to generate superlattice potential in the  $n$ -layer graphene. As is illustrated in Fig. 3, we have  $n$ -layer graphene separated with a twisted bilayer graphene (TBG) by a thin hBN with thickness  $d$ . TBG has moiré lattice constant  $a_M = a_G / (2 \sin \frac{\theta}{2})$  controlled by its twist angle  $\theta$ . The Coulomb interaction between the TBG layer and the  $n$ -layer graphene will effectively induce a moiré potential in the  $n$ -layer graphene layers. We will fix the density of the TBG to be  $\nu_{\text{TBG}} = 4$  so it is in a band insulator. Then the TBG has a charge profile, which generates superlattice potential felt by each layer of the  $n$ -layer graphene:  $V_l(\mathbf{G}_i) = \frac{2}{\sqrt{3}} \frac{e^2}{2\epsilon\epsilon_0 a_M} e^{-G_M(d+ld_{\text{layer}})} \frac{1}{G_M a_M} \langle \rho(\mathbf{G}_M) \rangle$ , where  $\langle \rho(\mathbf{G}_M) \rangle$  is the Fourier transformation of the density profile in the TBG and  $d_{\text{layer}} = 0.34\text{nm}$  is the distance between the adjacent graphene layers.  $l = 0, 1, \dots$  is the layer index count from the one closest to the TBG. The Hamiltonian also depends on the rotation angle of the  $n$ -layer graphene relative to the TBG through the  $\theta_3$  term

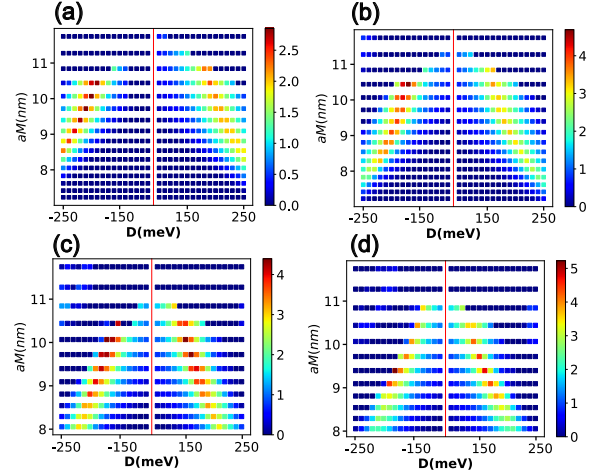


FIG. 4: Dependence of  $\frac{|C|\Delta}{W}$  on  $D$  and  $a_M$  of the  $n$ -layer graphene/hBN/TBG setup for (a) 4-layer, (b) 5-layer, (c) 6-layer, (d) 7-layer.  $|C|$ ,  $\Delta$  and  $W$  follow the same definition as in Fig. 2(a). Here we use  $\epsilon = 6$ , and the distance between the TBG and  $n$ -layer graphene is  $d = 1\text{nm}$ .

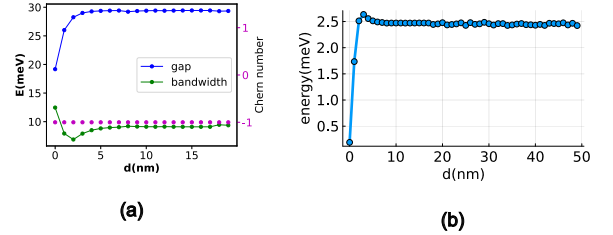


FIG. 5: (a) The band gap, the bandwidth and Chern number for the 5-layer graphene/hBN/TBG system at filling  $\nu = 1$  as a function of the distance  $d$  between the TBG and 5-layer graphene in the setup of Fig. 3. Here we use  $D = 180\text{meV}$ . (b) Many body gap for  $D = 180\text{meV}$ , at  $\nu = \frac{2}{3}$  with system size  $4 \times 6$ . We use twisted angle  $\theta = 1.5^\circ$  ( $a_M \approx 9.4\text{nm}$ ), and dielectric constant  $\epsilon = 6$ . One can see that FQAH is possible now also at the  $D > 0$  side and survives to the  $d \rightarrow +\infty$  limit.

in Eq. 1. For now we set  $\theta_3 = 0$  for simplicity.

**Narrow  $C = 1$  Chern band in the  $n$ -layer graphene/hBN/TBG system** We perform the Hartree Fock calculation and draw a phase diagram in Fig. 4. The result is quite similar to Fig. 2(a) of the 5-layer graphene/hBN system. We find that a narrow  $C = 1$  Chern band is possible for 4-layer, 5-layer, 6-layer and 7-layer graphene system with  $a_M$  in a range smaller than 11nm. Now the  $D > 0$  side also hosts a narrow Chern band. We can also replace TBG with a monolayer graphene (MG) aligned with the middle hBN. At  $d = 1\text{nm}$ , for  $\epsilon = 6$ , the moiré potentials

$V_0(G_M)$  in the n-layer graphene/hBN/TBG and n-layer graphene/hBN/MG are, 17.9meV and 0.84meV, respectively. In our Hartree Fock calculation we can get the QAH Wigner crystal in both cases as the moiré potential does not make any difference. But it is known that the Hartree Fock calculation may overestimate the strength of an insulating state, we leave to future experiment to see whether the weak moiré potential from the n-layer graphene/hBN/MG system is enough to stabilize the QAH crystal and FQAH phases. In this new setup we can control the moiré potential by tuning the distance  $d$ . In Fig. 5, we find that QAH-Wigner crystal phase, together with the FQAH phase, survive to the  $d \rightarrow +\infty$  limit also for  $D > 0$ , consistent with our conclusion that the external moiré potential is not essential for the Chern band physics.

**Summary** In conclusion, we studied the recently observed FQAH in the pentalayer rhombohedral stacked graphene aligned with hBN and in related systems. In contrast to the standard framework for other moiré systems, we find that the external moiré potential is negligible and the QAH and FQAH phases should be understood as from a spontaneously formed topological Wigner crystal due to interaction in a model with continuous translation symmetry. In future it is interesting to study the interplay between the almost gapless phonon modes of the Wigner crystal with the small moiré potential and disorder. As the QAH Wigner crystal is stabilized with a

period around 10nm, it may be possible to stabilize it at  $\nu = 1/2$  filling of moiré unit cell with a moiré lattice constant of around 5nm. Besides, we propose a new setup with moiré in the n-layer graphene generated from the Coulomb repulsion of twist bilayer graphene separated by a thin hBN. We find similar narrow  $C = 1$  Chern band in  $n_{\text{layer}} = 4, 5, 6, 7$ . The ability to separately tune the superlattice potential and the moiré period should reveal a rich phase diagram in future experimental studies. It is also interesting to dope the TBG layer, which screens the Coulomb in the n-layer graphene and may drive a transition out of the quantum Hall phases[62].

*Note added:* We note two other papers[63, 64] on the same topic also appeared roughly at the same time. Our results agree with each other when they overlap.

**Acknowledgement** YHZ thanks Zhihuan Dong and T. Senthil for many inspiring discussions and previous collaborations on moiré systems. We especially thank Zhihuan Dong for helps on improving the efficiency of the Hartree Fock calculation. We also thank Long Ju and Sankar Das Sarma for discussions and useful comments. The numerical simulation was carried out at the Advanced Research Computing at Hopkins (ARCH) core facility (rockfish.jhu.edu), which is supported by the National Science Foundation (NSF) grant number OAC 1920103. This work was supported by the National Science Foundation under Grant No. DMR-2237031.

- 
- [1] H. L. Stormer, D. C. Tsui, and A. C. Gossard, *Reviews of Modern Physics* **71**, S298 (1999).
- [2] J. K. Jain, *Physical review letters* **63**, 199 (1989).
- [3] K. Sun, Z. Gu, H. Katsura, and S. D. Sarma, *Physical review letters* **106**, 236803 (2011).
- [4] D. Sheng, Z.-C. Gu, K. Sun, and L. Sheng, *Nature communications* **2**, 389 (2011).
- [5] T. Neupert, L. Santos, C. Chamon, and C. Mudry, *Physical review letters* **106**, 236804 (2011).
- [6] Y.-F. Wang, Z.-C. Gu, C.-D. Gong, and D. Sheng, *Physical review letters* **107**, 146803 (2011).
- [7] E. Tang, J.-W. Mei, and X.-G. Wen, *Physical review letters* **106**, 236802 (2011).
- [8] N. Regnault and B. A. Bernevig, *Physical Review X* **1**, 021014 (2011).
- [9] E. J. Bergholtz and Z. Liu, *International Journal of Modern Physics B* **27**, 1330017 (2013).
- [10] S. A. Parameswaran, R. Roy, and S. L. Sondhi, *Comptes Rendus Physique* **14**, 816 (2013).
- [11] T. Neupert, L. Santos, S. Ryu, C. Chamon, and C. Mudry, *Phys. Rev. B* **84**, 165107 (2011).
- [12] E. M. Spanton, A. A. Zibrov, H. Zhou, T. Taniguchi, K. Watanabe, M. P. Zaletel, and A. F. Young, *Science* **360**, 62 (2018).
- [13] Y. Xie, A. T. Pierce, J. M. Park, D. E. Parker, E. Khalaf, P. Ledwith, Y. Cao, S. H. Lee, S. Chen, P. R. Forrester, *et al.*, *Nature* **600**, 439 (2021).
- [14] Y.-H. Zhang, D. Mao, Y. Cao, P. Jarillo-Herrero, and T. Senthil, *Physical Review B* **99**, 075127 (2019).
- [15] P. J. Ledwith, G. Tarnopolsky, E. Khalaf, and A. Vishwanath, *Physical Review Research* **2**, 023237 (2020).
- [16] C. Repellin and T. Senthil, *Physical Review Research* **2**, 023238 (2020).
- [17] A. Abouelkomsan, Z. Liu, and E. J. Bergholtz, *Physical review letters* **124**, 106803 (2020).
- [18] P. Wilhelm, T. C. Lang, and A. M. Läuchli, *Physical Review B* **103**, 125406 (2021).
- [19] C. Repellin, Z. Dong, Y.-H. Zhang, and T. Senthil, *Physical Review Letters* **124**, 187601 (2020).
- [20] A. L. Sharpe, E. J. Fox, A. W. Barnard, J. Finney, K. Watanabe, T. Taniguchi, M. Kastner, and D. Goldhaber-Gordon, *Science* **365**, 605 (2019).
- [21] M. Serlin, C. Tschirhart, H. Polshyn, Y. Zhang, J. Zhu, K. Watanabe, T. Taniguchi, L. Balents, and A. Young, *Science* **367**, 900 (2020).
- [22] Y.-H. Zhang, D. Mao, and T. Senthil, *Physical Review Research* **1**, 033126 (2019).
- [23] N. Bultinck, S. Chatterjee, and M. P. Zaletel, *Physical review letters* **124**, 166601 (2020).
- [24] G. Chen, A. L. Sharpe, E. J. Fox, Y.-H. Zhang, S. Wang, L. Jiang, B. Lyu, H. Li, K. Watanabe, T. Taniguchi, *et al.*, *Nature* **579**, 56 (2020).
- [25] T. Li, S. Jiang, B. Shen, Y. Zhang, L. Li, Z. Tao, T. Devakul, K. Watanabe, T. Taniguchi, L. Fu, *et al.*, *Nature* **600**, 641 (2021).
- [26] B. A. Foutty, C. R. Kometter, T. Devakul, A. P. Reddy, K. Watanabe, T. Taniguchi, L. Fu, and B. E. Feldman, *arXiv preprint arXiv:2304.09808* (2023).

- [27] J. Cai, E. Anderson, C. Wang, X. Zhang, X. Liu, W. Holtzmann, Y. Zhang, F. Fan, T. Taniguchi, K. Watanabe, Y. Ran, T. Cao, L. Fu, D. Xiao, W. Yao, and X. Xu, *Nature* (2023), [10.1038/s41586-023-06289-w](https://doi.org/10.1038/s41586-023-06289-w).
- [28] Y. Zeng, Z. Xia, K. Kang, J. Zhu, P. Knüppel, C. Vaswani, K. Watanabe, T. Taniguchi, K. F. Mak, and J. Shan, *Nature* (2023), [10.1038/s41586-023-06452-3](https://doi.org/10.1038/s41586-023-06452-3).
- [29] H. Park, J. Cai, E. Anderson, Y. Zhang, J. Zhu, X. Liu, C. Wang, W. Holtzmann, C. Hu, Z. Liu, T. Taniguchi, K. Watanabe, J.-h. Chu, T. Cao, L. Fu, W. Yao, C.-Z. Chang, D. Cobden, D. Xiao, and X. Xu, *Nature* (2023), [10.1038/s41586-023-06536-0](https://doi.org/10.1038/s41586-023-06536-0).
- [30] F. Xu, Z. Sun, T. Jia, C. Liu, C. Xu, C. Li, Y. Gu, K. Watanabe, T. Taniguchi, B. Tong, J. Jia, Z. Shi, S. Jiang, Y. Zhang, X. Liu, and T. Li, *Phys. Rev. X* **13**, 031037 (2023).
- [31] F. Wu, T. Lovorn, E. Tutuc, I. Martin, and A. MacDonald, *Physical review letters* **122**, 086402 (2019).
- [32] H. Yu, M. Chen, and W. Yao, *National Science Review* **7**, 12 (2020).
- [33] T. Devakul, V. Crépel, Y. Zhang, and L. Fu, *Nature communications* **12**, 6730 (2021).
- [34] H. Li, U. Kumar, K. Sun, and S.-Z. Lin, *Physical Review Research* **3**, L032070 (2021).
- [35] V. Crépel and L. Fu, *Phys. Rev. B* **107**, L201109 (2023).
- [36] C. Wang, X.-W. Zhang, X. Liu, Y. He, X. Xu, Y. Ran, T. Cao, and D. Xiao, *arXiv preprint arXiv:2304.11864* (2023).
- [37] A. P. Reddy, F. F. Alsallom, Y. Zhang, T. Devakul, and L. Fu, *arXiv preprint arXiv:2304.12261* (2023).
- [38] C. Xu, J. Li, Y. Xu, Z. Bi, and Y. Zhang, *arXiv e-prints*, [arXiv:2308.09697](https://arxiv.org/abs/2308.09697) (2023), [arXiv:2308.09697](https://arxiv.org/abs/2308.09697) [cond-mat.str-el].
- [39] J. Yu, J. Herzog-Arbeitman, M. Wang, O. Vafek, B. A. Bernevig, and N. Regnault, *arXiv e-prints*, [arXiv:2309.14429](https://arxiv.org/abs/2309.14429) (2023), [arXiv:2309.14429](https://arxiv.org/abs/2309.14429) [cond-mat.mes-hall].
- [40] H. Goldman, A. P. Reddy, N. Paul, and L. Fu, *Phys. Rev. Lett.* **131**, 136501 (2023).
- [41] J. Dong, J. Wang, P. J. Ledwith, A. Vishwanath, and D. E. Parker, *Phys. Rev. Lett.* **131**, 136502 (2023).
- [42] P. J. Ledwith, A. Vishwanath, and E. Khalaf, *Physical Review Letters* **128**, 176404 (2022).
- [43] J. Wang and Z. Liu, *Physical Review Letters* **128**, 176403 (2022).
- [44] T. Devakul, P. J. Ledwith, L.-Q. Xia, A. Uri, S. C. de la Barrera, P. Jarillo-Herrero, and L. Fu, *Science Advances* **9**, eadi6063 (2023).
- [45] J. Wang, S. Klevtsov, and Z. Liu, *Physical Review Research* **5**, 023167 (2023).
- [46] Q. Gao, J. Dong, P. Ledwith, D. Parker, and E. Khalaf, *Physical Review Letters* **131**, 096401 (2023).
- [47] S. A. A. Ghorashi, A. Dunbrack, A. Abouelkomsan, J. Sun, X. Du, and J. Cano, *Physical Review Letters* **130**, 196201 (2023).
- [48] Z. Lu, T. Han, Y. Yao, A. P. Reddy, J. Yang, J. Seo, K. Watanabe, T. Taniguchi, L. Fu, and L. Ju, *arXiv e-prints*, [arXiv:2309.17436](https://arxiv.org/abs/2309.17436) (2023), [arXiv:2309.17436](https://arxiv.org/abs/2309.17436) [cond-mat.mes-hall].
- [49] Y.-H. Zhang and T. Senthil, *Physical Review B* **99**, 205150 (2019).
- [50] A. Kumar and R. Nandkishore, *Phys. Rev. B* **87**, 241108 (2013).
- [51] B. I. Halperin, P. A. Lee, and N. Read, *Physical Review B* **47**, 7312 (1993).
- [52] H. Zhou, T. Xie, A. Ghazaryan, T. Holder, J. R. Ehrets, E. M. Spanton, T. Taniguchi, K. Watanabe, E. Berg, M. Serbyn, *et al.*, *Nature* **598**, 429 (2021).
- [53] A. S. Patri and T. Senthil, *Physical Review B* **107**, 165122 (2023).
- [54] T. Han, Z. Lu, G. Scuri, J. Sung, J. Wang, T. Han, K. Watanabe, T. Taniguchi, H. Park, and L. Ju, *arXiv preprint arXiv:2305.03151* (2023).
- [55] T. Han, Z. Lu, Y. Yao, J. Yang, J. Seo, C. Yoon, K. Watanabe, T. Taniguchi, L. Fu, F. Zhang, *et al.*, *arXiv preprint arXiv:2310.17483* (2023).
- [56] T. Han, Z. Lu, G. Scuri, J. Sung, J. Wang, T. Han, K. Watanabe, T. Taniguchi, L. Fu, H. Park, *et al.*, *Nature*, 1 (2023).
- [57] K. Liu, J. Zheng, Y. Sha, B. Lyu, F. Li, Y. Park, Y. Ren, K. Watanabe, T. Taniguchi, J. Jia, *et al.*, *arXiv preprint arXiv:2306.11042* (2023).
- [58] A. M. Seiler, F. R. Geisenhof, F. Winterer, K. Watanabe, T. Taniguchi, T. Xu, F. Zhang, and R. T. Weitz, *Nature* **608**, 298 (2022).
- [59] Y. Park, Y. Kim, B. L. Chittari, and J. Jung, *Phys. Rev. B* **108**, 155406 (2023), [arXiv:2304.12874](https://arxiv.org/abs/2304.12874) [cond-mat.mes-hall].
- [60] F. Zhang, B. Sahu, H. Min, and A. H. MacDonald, *Phys. Rev. B* **82**, 035409 (2010).
- [61] J. Jung, A. Raoux, Z. Qiao, and A. H. MacDonald, *Phys. Rev. B* **89**, 205414 (2014).
- [62] X.-Y. Song, Y.-H. Zhang, and T. Senthil, *arXiv preprint arXiv:2308.10903* (2023).
- [63] Z. Dong, A. S. Patri, and T. Senthil, “Theory of fractional quantum anomalous hall phases in pentagonal rhombohedral graphene moiré structures,” (2023), [arXiv:2311.03445](https://arxiv.org/abs/2311.03445) [cond-mat.str-el].
- [64] J. Dong, T. Wang, T. Wang, T. Soejima, M. P. Zaletel, A. Vishwanath, and D. E. Parker, “Anomalous hall crystals in rhombohedral multilayer graphene i: Interaction-driven chern bands and fractional quantum hall states at zero magnetic field,” (2023), [arXiv:2311.05568](https://arxiv.org/abs/2311.05568) [cond-mat.str-el].

## Appendix A: The moiré potential form

The moiré potential parameters used in our calculation are listed in the following:

$$\begin{aligned} H_z(\mathbf{G}_1) &= H_z(\mathbf{G}_3) = H_z(\mathbf{G}_5) = C_z e^{i\phi_z} \\ &= H_z^*(\mathbf{G}_2) = H_z^*(\mathbf{G}_4) = H_z^*(\mathbf{G}_6), \end{aligned} \quad (\text{A1})$$

$$\begin{aligned} H_0(\mathbf{G}_1) &= H_0(\mathbf{G}_3) = H_0(\mathbf{G}_5) = C_0 e^{i\phi_0} \\ &= H_0^*(\mathbf{G}_2) = H_0^*(\mathbf{G}_4) = H_0^*(\mathbf{G}_6), \end{aligned} \quad (\text{A2})$$

$$H_{AB}(\mathbf{G}_1) = H_{AB}^*(\mathbf{G}_4) = C_{AB} e^{i(2\pi/3 - \phi_{AB})}, \quad (\text{A3})$$

$$H_{AB}(\mathbf{G}_3) = H_{AB}^*(\mathbf{G}_2) = C_{AB} e^{-i\phi_{AB}}, \quad (\text{A4})$$

$$H_{AB}(\mathbf{G}_5) = H_{AB}^*(\mathbf{G}_6) = C_{AB} e^{i(-2\pi/3 - \phi_{AB})}, \quad (\text{A5})$$

where  $C_0 = -10.13\text{meV}$ ,  $\phi_0 = 86.53^\circ$ ,  $C_z = -9.01\text{meV}$ ,  $\phi_z = 8.43^\circ$ ,  $C_{AB} = 11.34\text{meV}$ ,  $\phi_{AB} = 19.60^\circ$ . Here  $H_{AA}(\mathbf{G}_j) = H_0(\mathbf{G}_j) + H_z(\mathbf{G}_j)$  and  $H_{BB}(\mathbf{G}_j) = H_0(\mathbf{G}_j) - H_z(\mathbf{G}_j)$  for each  $\mathbf{G}_j$ .

### Appendix B: Hartree Fock calculation

We perform Hartree Fock approximation by keeping the first  $N_b$  conduction bands in the MBZ. The interaction term is written as:

$$H_V = \frac{1}{2A} \sum_{\mathbf{q}} \sum_{l,l'} V_{l,l'}(\mathbf{q}) : \rho_l(\mathbf{q}) \rho_{l'}(-\mathbf{q}) :, \quad (\text{B1})$$

where  $\rho_l(\mathbf{q}) = \sum_{\mathbf{k},m,m'} c_m^\dagger(\mathbf{k} + \mathbf{q}) \Lambda_{m,m'}^l(\mathbf{k}, \mathbf{q}) c_{m'}(\mathbf{k})$  and  $\Lambda_{m,m'}^l(\mathbf{k}, \mathbf{q}) = \langle u_m(\mathbf{k} + \mathbf{q}) | P_l | u_{m'}(\mathbf{k}) \rangle$ ,  $P_l$  is the projection operator to layer  $l$ ,  $m$  and  $m'$  are band indices.  $V_{l,l'}(\mathbf{q}) = \frac{e^2 e^{-q|l-l'|d_{\text{layer}}} \tanh(q\lambda)}{2\epsilon\epsilon_0|q|}$ , where  $d_{\text{layer}}$  is the distance between nearest two layers,  $\lambda$  is the screening length. In our calculation, we choose that  $d_{\text{layer}} = 0.34\text{nm}$  and  $\lambda = 30\text{nm}$ . The interaction can be decoupled into Hartree and Fock terms respectively, leading to a mean field theory:

$$\begin{aligned} H_V &= \sum_{\mathbf{k}_1, \mathbf{k}_2} \sum_{\mathbf{q}} \sum_{m,m',n,n'} V_{m,m',n,n'}(\mathbf{k}_1, \mathbf{k}_2, \mathbf{q}) c_m^\dagger(\mathbf{k}_1 + \mathbf{q}) c_n^\dagger(\mathbf{k}_2 - \mathbf{q}) c_{n'}(\mathbf{k}_2) c_{m'}(\mathbf{k}_1) \\ &= \sum_{\mathbf{k}_1, \mathbf{k}_2} \sum_{m,m',n,n'} (V_{m,m',n,n'}(\mathbf{k}_1, \mathbf{k}_2, \mathbf{0}) - V_{m,m',m,n'}(\mathbf{k}_1, \mathbf{k}_2, \mathbf{k}_2 - \mathbf{k}_1)) \langle c_m^\dagger(\mathbf{k}_1) c_{m'}(\mathbf{k}_1) \rangle c_n^\dagger(\mathbf{k}_2) c_{n'}(\mathbf{k}_2). \end{aligned} \quad (\text{B2})$$

The interaction vertex  $V_{m,m',n,n'}(\mathbf{k}_1, \mathbf{k}_2, \mathbf{q})$  can be calculated as:

$$V_{m,m',n,n'}(\mathbf{k}_1, \mathbf{k}_2, \mathbf{q}) = \sum_{l,l'} V_{l,l'}(\mathbf{q}) \Lambda_{m,m'}^l(\mathbf{k}_1, \mathbf{q}) \Lambda_{n,n'}^l(\mathbf{k}_2, -\mathbf{q}). \quad (\text{B3})$$

In the above  $m, m', n, n' = 1, 2, \dots, N_b$  are the band indexes. In the calculation we solve  $\rho_{mm'}(\mathbf{k}) = \langle c_m^\dagger(\mathbf{k}) c_{m'}(\mathbf{k}) \rangle$  self consistently from randomized initial ansatz. We try 40 number of randomized initial ansatz and choose the one with lowest energy.

### Appendix C: ED calculation

We perform all the ED calculation in the hole picture. We use  $h(k)$  as the hole annihilation operator. The total Hamiltonian is written as:

$$H = - \sum_{\mathbf{k}} \epsilon_{\text{HF}}(\mathbf{k}) h^\dagger(\mathbf{k}) h(\mathbf{k}) + \sum_{\mathbf{k}_1, \mathbf{k}_2, \mathbf{q}} V(\mathbf{k}_1, \mathbf{k}_2, \mathbf{q}) h^\dagger(\mathbf{k}_1 + \mathbf{q}) h^\dagger(\mathbf{k}_2 - \mathbf{q}) h(\mathbf{k}_2) h(\mathbf{k}_1), \quad (\text{C1})$$

where  $\epsilon_{\text{HF}}(\mathbf{k})$  is the first conduction band dispersion after HF calculation. The interaction vertex can be calculated as:

$$V(\mathbf{k}_1, \mathbf{k}_2, \mathbf{q}) = \sum_{l,l'} V_{l,l'}(\mathbf{q}) \left( \Lambda_{\text{HF}}^l(\mathbf{k}_1, \mathbf{q}) \Lambda_{\text{HF}}^{l'}(\mathbf{k}_2, -\mathbf{q}) \right)^*, \quad (\text{C2})$$

where  $\Lambda_{\text{HF}}^l(\mathbf{k}_1, \mathbf{q}) = \langle u_{\text{HF}}(\mathbf{k}_1 + \mathbf{q}) | P_l | u_{\text{HF}}(\mathbf{k}_1) \rangle$  is the form factor of the bloch wavefunction on layer  $l$  after performing HF approximation.

### Appendix D: Composite Fermi liquid at $\nu = 1/2$ filling

With parameters  $\theta = 0.9^\circ$  ( $a_M = 10.63\text{nm}$ ),  $\epsilon = 6$ ,  $D = -160\text{meV}$ , we perform an ED calculation at  $\nu = 1/2$  filling in system size of  $4 \times 5$  and  $4 \times 6$ . The result is shown in Fig. 6. In  $4 \times 5$  size case, we perform a HF calculation at a  $20 \times 20$  system and extracts a  $4 \times 5$  submesh to perform the ED calculation. In  $4 \times 6$  case, we perform a HF calculation at a  $24 \times 24$  system and extracts a  $4 \times 6$  submesh to perform the ED calculation. As shown in Fig. 6, we do not see any many body gap in the ED spectrum, implying a gapless state. Meanwhile the momentum distribution  $n(\mathbf{k})$  is relatively flat. Therefore the phase is consistent with the composite Fermi liquid (CFL) state.

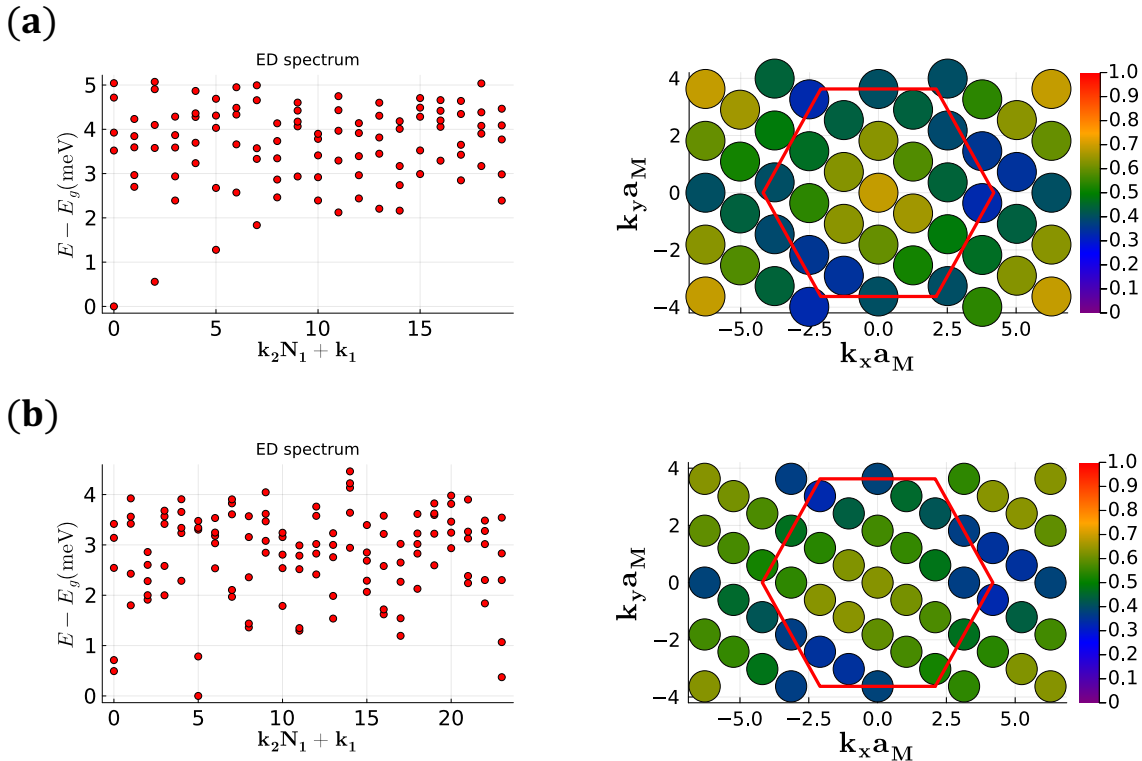


FIG. 6: (a) ED calculation at  $\nu = 1/2$  filling with system size of  $4 \times 5$  and the momentum distribution  $n(\mathbf{k} = \langle c^\dagger(\mathbf{k})c(\mathbf{k}) \rangle)$ . (b) Similar with (a), but the system size is  $4 \times 6$  instead.

### Appendix E: More results

We use  $N_b = 3$  to perform the Hartree Fock calculation in the main text, in which the bare band structure is obtained by using free electron approximation in  $5 \times 5$  moiré Brillouin zones. We also do HF calculation in  $N_b = 4, 5$  cases, the result is shown in Fig. 7. It is verified that the many body gap have already converged at  $N_b = 3$ . At  $\epsilon = 6$  and  $N_b = 4$ , dependence of  $\frac{|C|\Delta}{W}$  on  $D$  and  $a_M$  is shown in Fig. 8(d), which is nearly the same as Fig.2(a) in the main text.

We also add more details about Fig.2(a) in the main text in Fig. 8(a)-(c).

### Appendix F: The moiré potential from TBG or MG

We consider a different way to generate the moiré potential in the  $n$ -layer graphene through Coulomb interaction. We separate it with twisted bilayer graphene (TBG) or monolayer graphene (aligned with the middle hBN) through a thin hBN with thickness  $d$ . The coulomb interaction between TBG (or monolayer graphene) and the graphene layers



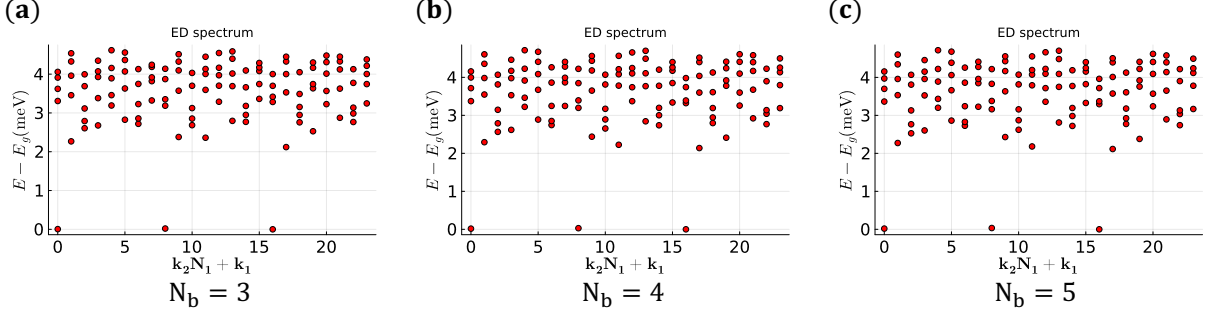


FIG. 7: ED calculation of the 5-layer graphene/hBN system at  $\theta = 0.77^\circ$  ( $a_M = 11.36\text{nm}$ ),  $\epsilon = 6$ ,  $D = -160\text{meV}$ . The system size is fixed to be  $4 \times 6$ .

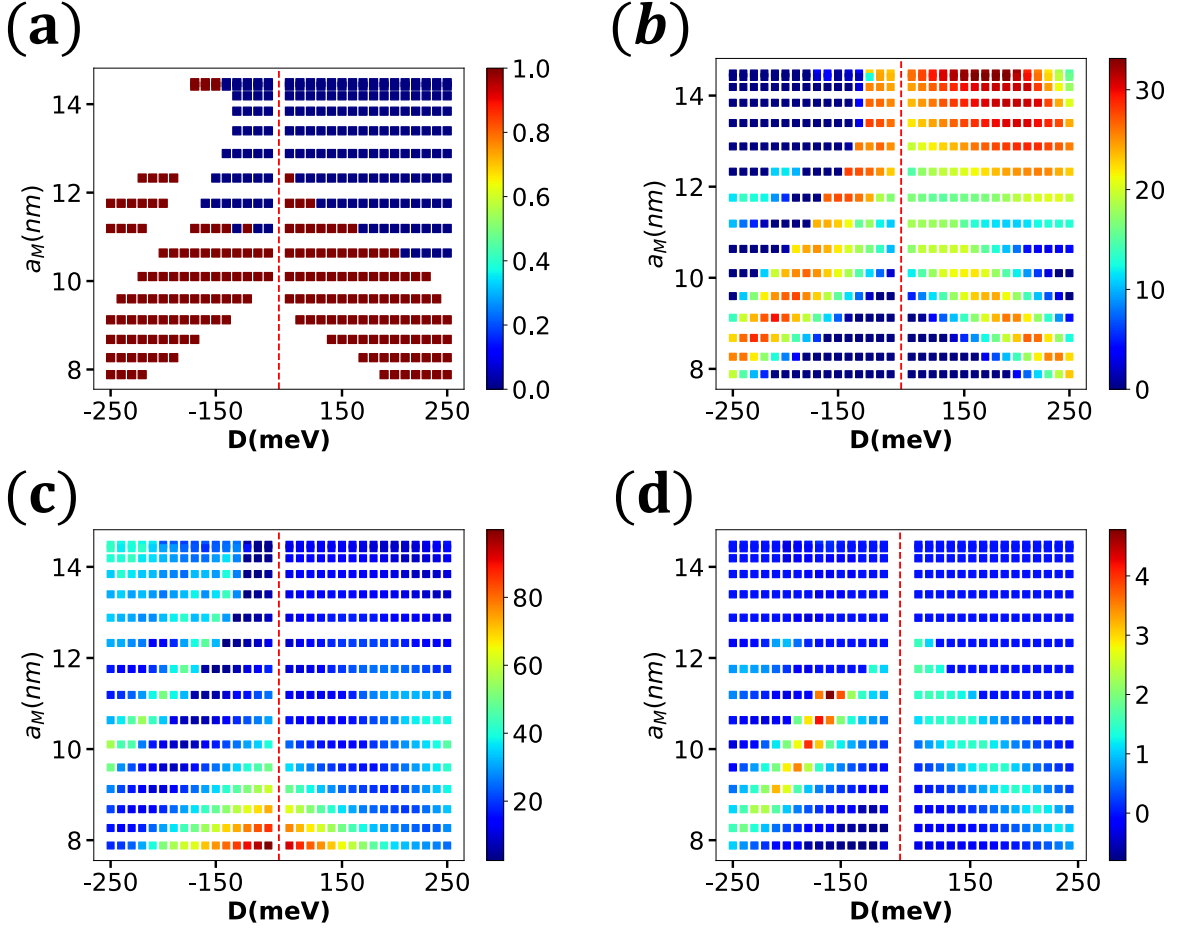


FIG. 8: The same parameters as in Fig.2(a) in the main text, but in (d) we use  $N_b = 4$  instead. In (a)-(c), we still use  $N_b = 3$ . (a) Absolute value of lowest band's Chern number after HF:  $|C|$ . The blank area corresponds to the metal phase. (b) The band gap after HF:  $\Delta$ . (c) The band width of the lowest band after HF:  $W$ . (d)  $\frac{|C|\Delta}{W}$ .

is:

$$H_V = \frac{1}{A} \sum_{\mathbf{q}, l} V_l(\mathbf{q}) \rho_{t,l}(\mathbf{q}) \rho_b(-\mathbf{q}), \quad (\text{F1})$$

where  $\rho_b(\mathbf{q}) = \sum_{\mathbf{k}} f_b^\dagger(\mathbf{k} + \mathbf{q}) f_b(\mathbf{k})$  and  $\rho_{t,l}(-\mathbf{q}) = \sum_{\mathbf{k}} f_{t,l}^\dagger(\mathbf{k} - \mathbf{q}) f_{t,l}(\mathbf{k})$  correspond to the density in the twisted bilayer graphene, and the density in each layer in the multilayer graphene respectively.  $A = \frac{4\pi^2 N_{\text{cell}}}{|\mathbf{G}_1 \times \mathbf{G}_2|}$  is the sample

area.  $V_l(\mathbf{q}) = \frac{e^2}{2\epsilon\epsilon_0|\mathbf{q}|}e^{-|\mathbf{q}|(d+ld_{\text{layer}})}$  is the screened Coulomb potential in the materials, and  $\epsilon$  is the dielectric constant,  $d_{\text{layer}}$  is the interlayer distance of the graphene multilayers. In the discretized momentum space, the interaction  $H_V$  becomes:

$$\begin{aligned} H_V &= \frac{2}{\sqrt{3}} \frac{1}{N_{\text{cell}}} \sum_{\mathbf{q},l} \frac{e^2}{2\epsilon\epsilon_0 a_M} \frac{1}{|\mathbf{q}| a_M} e^{-|\mathbf{q}|(d+ld_{\text{layer}})} \rho_b(\mathbf{q}) \rho_{t,l}(-\mathbf{q}) \\ &= \frac{2}{\sqrt{3}} \frac{1}{N_{\text{cell}}} \sum_{\mathbf{q},l} \frac{e^2}{2\epsilon\epsilon_0 a_M} \frac{1}{|\mathbf{q}| a_M} e^{-|\mathbf{q}|(d+ld_{\text{layer}})} \rho_b(\mathbf{q}) \sum_{\mathbf{k}_2} f_{t,l}^\dagger(\mathbf{k}_2 - \mathbf{q}) f_{t,l}(\mathbf{k}_2). \end{aligned} \quad (\text{F2})$$

The density in the twisted bilayer graphene can be approximated as:

$$\rho_b(\mathbf{q}) = \sum_{\mathbf{k}} c_b^\dagger(\mathbf{k} + \mathbf{q}) \Lambda_b(\mathbf{k}, \mathbf{q}) c_b(\mathbf{k}), \quad (\text{F3})$$

where  $\Lambda_b(\mathbf{k}, \mathbf{q}) = \langle u_b(\mathbf{k} + \mathbf{q}) | u_b(\mathbf{k}) \rangle$  is the form factor,  $c_b(\mathbf{k})$  is the annihilation operator of the electrons in the conduction band. The potential generated to the  $n$ -layer graphene is:

$$V_l(\mathbf{G}_M) = \frac{2}{\sqrt{3}} \frac{e^2}{2\epsilon\epsilon_0 a_M} e^{-G_M(d+ld_{\text{layer}})} \frac{1}{G_M a_M} \langle \rho_b(\mathbf{G}_M) \rangle, \quad (\text{F4})$$

where  $d$  is also the distance between the TBG (or MG) and the closest layer of multilayer graphene. Finally, we find the potential in the layer  $l = 0, 1, \dots, n_{\text{layer}} - 1$  is  $V_l(\mathbf{G}_M) = V_0(\mathbf{G}_M) e^{-G_M l d_{\text{layer}}}$ , where  $V_0(\mathbf{G}_M)$  is the strength of the potential in the first graphene layer and it depends on the twisted angle and the distance between the hBN and the graphene layer.

We have shown the phase diagram for the case with TBG. We can also use monolayer graphene aligned with the middle hBN. But this time the density profile  $\rho_b(\mathbf{G}_M)$  is weaker by a factor of 10. At  $d = 1\text{nm}$  and  $\epsilon = 6$ , the moiré potential  $V_0(G_M)$  imprinted on the  $n$ -layer graphene is only around 0.8 meV. However, in our Hartree-Fock calculation, we still find robust region of narrow  $C = 1$  Chern band at  $\nu = 1$ , as shown in Fig.9. This is expected because the moiré potential is negligible and not essential anyway in our Hartree Fock calculation.

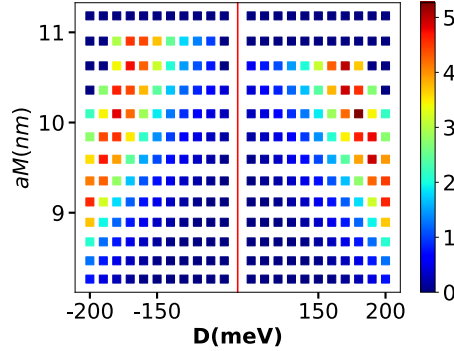


FIG. 9:  $\frac{|C|\Delta}{W}$  of 5-layer graphene/hBN/MG system.  $a_M$  is controlled by the twist angle of the MG and the middle hBN. We use  $\epsilon = 6$ ,  $d = 5\text{nm}$ .